

Watching Polarons Form in Real Time

Victor Garcia-Herrero,¹ Christoph Emeis,¹ Zhenbang Dai,² Jon Lafuente-Bartolome,^{3,4} Feliciano Giustino,^{2,4} and Fabio Caruso¹

¹*Institut für Theoretische Physik und Astrophysik,
Christian-Albrechts-Universität zu Kiel, Kiel, Germany*

²*Oden Institute for Computational Engineering and Sciences,
The University of Texas at Austin, Austin, TX 78712*

³*Department of Physics, University of the Basque Country UPV/EHU, 48940 Leioa, Basque Country, Spain*

⁴*Department of Physics, The University of Texas at Austin, Austin, TX 78712*

Polaron formation in pump-probe experiments is an inherently non-equilibrium phenomenon, driven by the ultrafast coupled dynamics of electrons and phonons, and culminating in the emergence of a localized quasiparticle state. In this work, we present a first-principles quantum-kinetic theory of polaron formation that captures the real-time evolution of electronic and lattice degrees of freedom in presence of electron-phonon coupling. We implement this framework to investigate the ultrafast polaron formation in the prototypical polar insulator MgO. This approach allows us to determine the characteristic timescales of polaron localization and to identify its distinctive dynamical fingerprint. Our results establish clear and experimentally accessible criteria for identifying polaron formation in pump-probe experiments.

Polarons are composite quasiparticles arising from the mutual localization of a charge carrier and a lattice distortion and represent one of the paradigmatic manifestations of electron-phonon physics in materials [1]. Polarons leave distinctive identifiable features across a variety of experimental techniques that probe crystals under static or quasi equilibrium conditions. Both small and large polarons exhibit clear fingerprints in temperature-dependent resistivity measurements [2, 3]. They further manifest in phenomena such as the Stokes shift and broad luminescence arising from self-trapped excitons [4]. More recently, real-space localization of polarons has been directly observed through scanning tunneling microscopy [5], and atomic force microscopy techniques [6].

The advent of ultrafast spectroscopy [7] and scattering techniques [8] is offering a powerful opportunity to probe polaron formation in real time [9–11], enabling the direct observation of the emergence of symmetry-breaking lattice distortions and carrier localization. The dynamical process of polaron formation, schematically illustrated in Fig. 1, is initiated by the introduction of an additional charge in the system – for example, via ultrafast charge transfer, photoabsorption, or threshold ionization [12, 13]. The transition from the delocalized high-symmetry state to a polaronic distorted structure requires a non-trivial dynamical and dissipative process, which entails (i) the conversion of potential energy into kinetic energy, initiating coherent lattice motion, [14] and (ii) the gradual loss of coherence through dissipation, ultimately stabilizing the polaronic ground state [15].

Conclusive identification of polaron formation in pump-probe experiments, however, remains challenging, owing to the difficulty of disentangling spectral fingerprints of polaronic from other dynamical processes, such as coherent phonons or electronic processes occurring on similar time and energy scales [16, 17]. These consider-

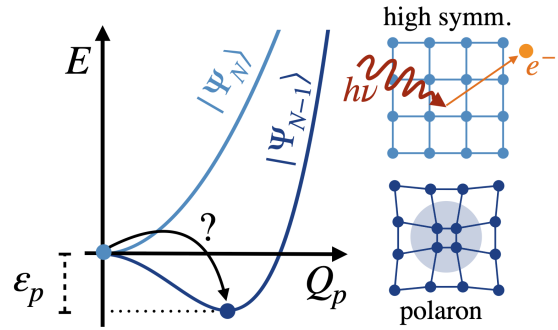


Figure 1. Schematic illustration of the ground-state potential energy surface E for an N - (light) and $N-1$ -electron systems (dark) as a function of Q_p – a generalized coordinate connecting the high-symmetry and the distorted polaronic structures. In the $N-1$ -electron system, polaron formation proceed via a dynamical process in which a structural distortion emerges in concomitance with carrier localization, resulting in an energy lowering by the polaron formation energy ε_p .

ations highlight the fundamental challenge of identifying distinctive dynamical fingerprints of polaron formation that may guide their systematic and conclusive identification in pump-probe experiments. While several theoretical and computational approach have been introduced and applied to describe polarons from first principles – including, e.g., hybrid density functional theory (DFT) [18, 19], perturbative many-body methods [20–22], self-consistent variational problems [23, 24], and Monte Carlo methods [25, 26] –, these approaches have thus far treated polarons as a static ground-state problem, which is not directly applicable to describe the polaron formation as a non-equilibrium problem in real time.

In this manuscript, we develop a quantum-kinetic approach to investigate the real-time dynamics of polaron formation from first principles. We apply it to investigate

the localization of electron and hole polarons in the polar insulators MgO. Our parameter-free simulations enable to predictively infer the characteristic timescales of polaron formation, its dynamical fingerprint, as well as the dissipative mechanisms at play. Overall, the polarons dynamics is accompanied by a electronic and structural oscillations with distinct soft frequency components that are absent in the ordinary phonon spectrum. This work thus identifies the distinctive dynamical blueprint of polarons, that may enable to conclusively distinguish them from other forms of structural motion (e.g., coherent phonons) thus guiding their identification in pump probe experiments. This work fills a critical gap in the theoretical modelling of the ultrafast polaron dynamics, and structural symmetry breaking in driven solids.

The structural distortions arising from the formation of a polaron are described by the operator $\Delta\hat{\tau}_{\kappa p}(t)$, which represents the displacement of the κ -th atom in the p -th unit cell relative to equilibrium. It can be expanded in a normal-mode basis as [27]: $\Delta\hat{\tau}_{\kappa p}(t) = -2N_p^{-1} \sum_{\mathbf{q}\nu} e^{i\mathbf{q}\mathbf{R}_p} (\hbar/2M_\kappa \omega_{\mathbf{q}\nu})^{1/2} \mathbf{e}_{\mathbf{q}\nu}^\kappa \hat{B}_{\mathbf{q}\nu}^*(t)$, where M_κ is the atomic mass, $\omega_{\mathbf{q}\nu}$ and $\mathbf{e}_{\mathbf{q}\nu}^\kappa$ are the frequency and eigenvector of a phonon with momentum \mathbf{q} and mode ν , respectively, \mathbf{R}_p is a crystal-lattice vector, and N_p the number of unit cells in Born-von-Karman periodic boundary conditions [27]. The expectation value $B_{\mathbf{q}\nu}(t) = \langle \hat{B}_{\mathbf{q}\nu}(t) \rangle$ is adimensional and quantifies the polaronic distortion of the lattice along the phonon $\mathbf{q}\nu$ [24].

The electronic counterpart of the polaron, quantifying the degree of localization of an additional charge in the system at time t , can be expressed via a wave-function *ansatz* $|\Psi(t)\rangle = |\Psi_{\text{el}}\rangle \otimes |\psi_p(t)\rangle$, where $|\Psi_{\text{el}}\rangle$ is the N -electron ground-state wave function, treated as time independent henceforth, and $|\psi_p(t)\rangle$ is the wave function of an extra electron or hole injected in the system at time $t = 0$. This *ansatz* is appropriate for the hole polaron in MgO investigated here since the system resides in the strong-coupling regime [22]. By introducing the expansion in Bloch basis $|\psi_p(t)\rangle = N_p^{-1/2} \sum_{n\mathbf{k}} A_{n\mathbf{k}}(t) |\psi_{n\mathbf{k}}\rangle$, – where $|\psi_{n\mathbf{k}}\rangle$ is the Bloch state for band n and crystal momentum \mathbf{k} – the degree of localization of the additional charge and its dynamics are fully specified by the set of complex time-dependent coefficients $A_{n\mathbf{k}}(t)$. Based on these definitions, the problem of polaron dynamics reduces to determining the time evolution of the phonon and electron envelope functions, $B_{\mathbf{q}\nu}(t)$ and $A_{n\mathbf{k}}(t)$, respectively.

To describe the dynamics of polaron formation, we derive a set of quantum kinetic equations for the time evolution of $\hat{B}_{\mathbf{q}\nu}(t)$. In Heisenberg picture, it obeys the equation of motion: $\partial^2 \hat{B}_{\mathbf{q}\nu} / \partial t^2 = -\hbar^{-2} [[\hat{B}_{\mathbf{q}\nu}, \hat{H}], \hat{H}]$. The lattice Hamiltonian $\hat{H} = \hat{H}_{\text{ph}} + \hat{H}_{\text{eph}}$ includes the harmonic phonon Hamiltonian \hat{H}_{ph} and the electron-phonon interaction \hat{H}_{eph} . We show in the Supplemental Materials [28] that by (i) evaluating the nested commutators

and (ii) taking the expectation value of fermionic operators within the adiabatic approximation using the polaron wave-function *ansatz* $|\Psi(t)\rangle$, one arrives at the following set of coupled equations:

$$\partial_t^2 B_{\mathbf{q}\nu} + \gamma_{\mathbf{q}\nu} \partial_t B_{\mathbf{q}\nu} + \omega_{\mathbf{q}\nu}^2 B_{\mathbf{q}\nu} = \frac{\omega_{\mathbf{q}\nu}}{\hbar N_p} \sum_{mn\mathbf{k}} g_{mn}^\nu(\mathbf{k}, \mathbf{q}) A_{m\mathbf{k}+\mathbf{q}}^* A_{n\mathbf{k}}, \quad (1)$$

$$[\varepsilon_{n\mathbf{k}} - \varepsilon] A_{n\mathbf{k}} = N_p^{-1} \sum_m \sum_{\mathbf{q}\nu} [g_{mn}^\nu(\mathbf{k}, \mathbf{q})]^* A_{m\mathbf{k}+\mathbf{q}} B_{\mathbf{q}\nu}, \quad (2)$$

where $\partial_t = \partial/\partial t$ and $\partial_t^2 = \partial^2/\partial t^2$, and $\gamma_{\mathbf{q}\nu}$ denotes the decoherence rate introduced according to Ref. [29]. $g_{nm}^\nu(\mathbf{k}, \mathbf{q})$ is the electron-phonon coupling matrix element and ε is polaron eigenvalue. Equation (2) is derived through variational minimization of the total electronic energy at time t with the constrained of preserving normalization ($N_p^{-1} \sum_{n\mathbf{k}} |A_{n\mathbf{k}}|^2 = 1$) [23]. This step corresponds to treat the electronic response to a time-dependent structural distortion within the adiabatic approximation. Equations (1) and (2) are the *time-dependent polaron equations* that can be solved by time propagation to infer the dynamics of the electron and phonon envelope functions, $A_{n\mathbf{k}}(t)$ and $B_{\mathbf{q}\nu}(t)$ throughout the polaron formation. A detailed derivation of this result is reported in the Supplemental Materials [28].

We implemented Eqs. (1) and (2) in a modified version of the EPW code [30] and applied them to investigate the polaron dynamics of the prototypical polar semiconductor MgO, for which polaron formation is well characterized in the ground state [18, 19, 31]. Electronic and vibrational properties are obtained from density-functional theory (DFT) and density functional perturbation theory calculations (DFPT) [32] as implemented in the plane-wave pseudo-potential code **Quantum Espresso** [33]. Equations (1) and (2) are solved on a homogeneous $24 \times 24 \times 24$ grid for \mathbf{k} and \mathbf{q} via second-order Runge-Kutta time stepping using a time stepping of 1 fs for a total simulation time of 4 ps. Further details on the numerical implementation and computational parameters are reported in the Supplemental Materials [28].

The polaron formation energy $E_p = \varepsilon + N_p^{-1} \sum_{\mathbf{q}\nu} |B_{\mathbf{q}\nu}|^2 \hbar \omega_{\mathbf{q}\nu}$ quantifies the energy gained by the crystal by forming a polaron following injection of a charge carrier. The time-dependent formation energy obtained from the solution of Eqs. (1) and (2) for MgO is reported in Fig. 2 (a) for time delays up to 1 ps following charge injection. At time $t = 0$, the extra charge is delocalized through the crystal and the structure undistorted, thus $E_p = 0$. For $t > 0$, E_p exhibits damped oscillations over timescales dictated by the longitudinal optical (LO) phonon period, indicating an oscillatory structural dynamics that accompanies the emergence of a polaron. Phonon-phonon interaction is the primary mechanisms for phonon decoherence in insulators [29], and it causes the damping of the

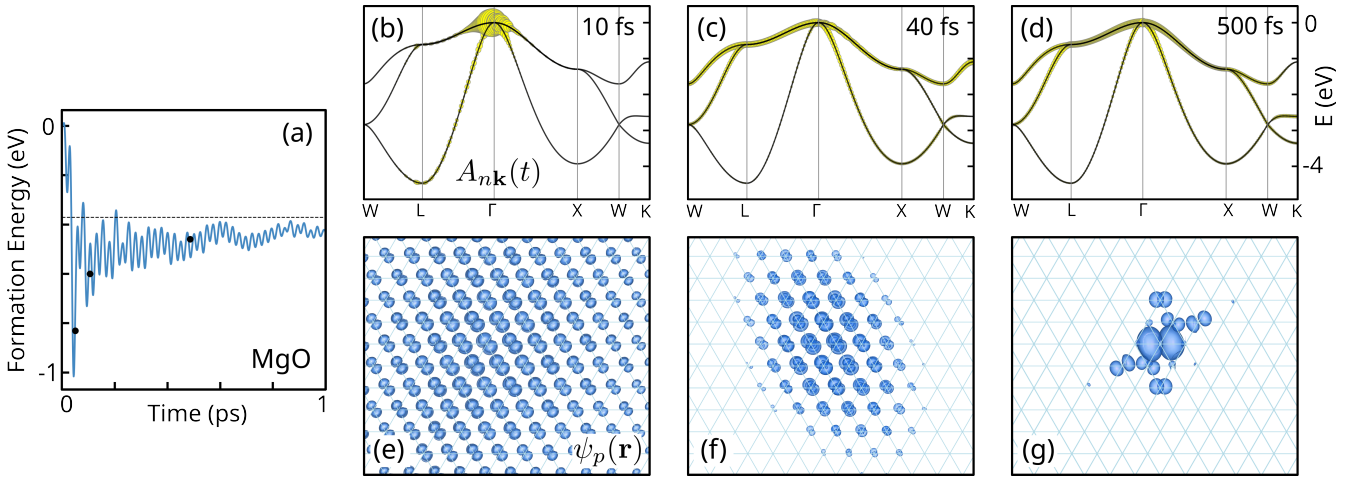


Figure 2. (a) Time dependence of the polaron formation energy throughout the dynamical formation of a hole polaron in MgO. The static polaron formation energy obtained from the solution of the static polaron equation or Ref. [24] is reported as dashed horizontal line. (b-d) Hole envelope function $A_{n\mathbf{k}}(t)$ obtained from the time propagation of the time-dependent polaron equations for time delays of $t = 10, 40$, and 500 fs, respectively (marked by black dots in panel (a)). (e-g) Density of an extra hole injected at the top of conduction band for the same time steps of panels (b-d).

oscillations within few picoseconds. After damping, we find $E_p(t = 5 \text{ ps}) \simeq -0.4 \text{ eV}$, which coincides with the static formation energy E_p^{static} [31] (marked by a dashed line in Fig. 2 (a)) obtained from the ground-state formalism developed in Refs. [23, 24]. Supplementary Fig. S1 further illustrates that static and dynamical formation energies agree for all choices of the \mathbf{k} -point meshes. This agreement demonstrates that once the polaron is fully formed, the dynamical results of Eqs. (1) and (2) converge to the established ground-state theory, thereby providing a consistency check that validates our simulations. To validate our approach and its numerical implementation, we conducted calculations of polaron formation within the DFT supercell formalism, with self-interaction correction based on Refs. Sadigh *et al.* [34] and Dai *et al.* [35]. Specifically, we considered a $10 \times 10 \times 10$ MgO supercell consisting of 2000 atoms, and compared polaron formation energy and electron densities at various timesteps along the non-equilibrium trajectories (Figs. S2 and S3 [28]). Overall, we find good agreement between the time-dependent polaron equations and DFT supercell calculations, confirming the correctness of the proposed framework.

To inspect the dynamics of charge localization, we report in Figs. 2 (b-d) the envelope function $A_{n\mathbf{k}}$ for time delays of $t = 10, 40$, and 500 fs, along a high-symmetry path in the Brillouin zone. Initially, $A_{n\mathbf{k}}$ is concentrated in the vicinity of the Γ high-symmetry point reflecting the delocalized character of the extra charge in real space. On longer times, the envelope function progressively spread out to encompass different momenta in the Brillouin zone, indicating the increased localization of the polaron charge density in real space. The localization process is further revealed by the isosurface plots of the

polaron wave function $\psi_p(\mathbf{r})$ – reported in Figs. 2 (e–f) at $t = 10, 40$, and 500 fs –, which indicate the emergence of distinct intermediate states of electronic localization during polaron formation. The full time dependence envelope function $A_{n\mathbf{k}}$ and of the polaron density is illustrated in the Supplementary Movies 1 and 2 [28]. In the SM, we further present results for the dynamical formation of large electron polarons in LiF (see supplementary discussion Section VII and Fig. S8 in [28]). In LiF, the polaron extends over a larger region of the lattice compared to the hole polaron in MgO, illustrating how the framework is capable of describing not only strongly localized polarons but also larger and more delocalized ones.

To illustrate the dynamics of the lattice distortion accompanying the polaron dynamics in MgO, we examine the time evolution of the phonon polaron envelope function $B_{\mathbf{q}\nu}(t)$, focusing on the LO mode ($\nu = \text{LO}$) and wave vectors \mathbf{q} along the W-L- Γ -X high-symmetry path in reciprocal space. $B_{\mathbf{q}\nu}(t)$ quantifies the displacement of the lattice along the phonon $\mathbf{q}\nu$ at time t , and it is thus a direct indicator of the structural motion. Its dynamics – illustrated in Fig. 3 (a) for the formation of a hole polarons and times up to 1 ps – exhibits pronounced oscillations across the entire Brillouin zone. The oscillation period varies significantly with momentum, increasing progressively as one moves away from the Γ point (Fig. 3 (c)). Wave vectors with larger oscillation amplitudes (darker color in Fig. 3 (a)) correspond to modes contributing more significantly to the overall polaronic distortion. Oscillations are damped within 1 ps (Fig. 3 (b)), suggesting that the polaron has formed within this time interval. A quantitative definition of the polaron formation time can be formulated by requiring that 90% of the atomics displacements for all atoms in the Born-von-Karman

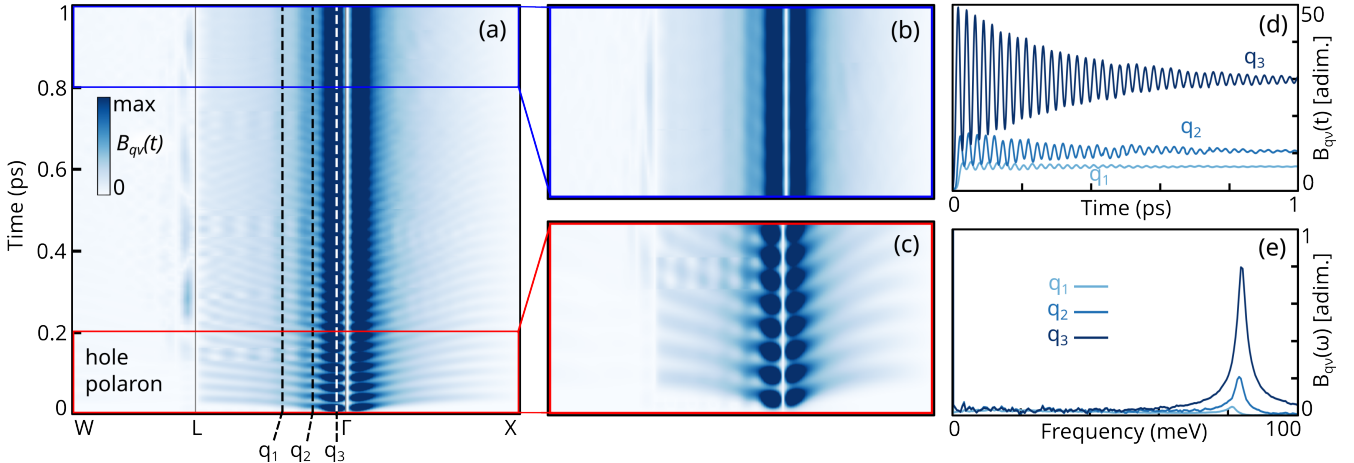


Figure 3. (a) Ultrafast modulation of the phonon polaron envelope function $B_{qv}(t)$ during the formation of a hole polaron in MgO. The phonon mode index ν is set to the longitudinal optical phonon, and the momentum \mathbf{q} runs along the W-L- Γ -X high-symmetry path in the Brillouin zone. (b-c) Enlarged views of the regions highlighted by the blue and red rectangles in panel (a). (d) Time dependence of the phonon envelope function $B_{qv}(t)$ for the momenta q_1, q_2, q_3 marked by vertical lines in panel (a). (e) Fourier transform $B_{qv}(\omega)$ of the data in (d).

supercell and relative to the final polaron structure fall below a threshold value of $\Delta_{th} = 0.005 \text{ \AA}$. Based on this criterion, we estimate the formation time for hole polarons in MgO to 0.8 ps (see Supplementary discussion V and Figs. S4 and S5 in [28]). This value agrees well with the characteristic timescales of polaron formation estimated via pump-probe optical experiments [15]. While no experimental data for dynamical polaron formation in MgO are available, existing time-resolved experiments for double perovskites [3, 36, 37] report polaron formation times ranging between 1 and 5 ps [37], matching closely the ones reported in our work. Overall, the timescale of polaron formation emerges as an intrinsic property of the material, determined by (i) the specific pathway connecting the distorted and undistorted structures, and (ii) the characteristic timescales of decoherence arising from phonon-phonon interactions. Conversely, the LO phonon period (~ 50 fs in MgO) does not play a significant role on these timescales. To further clarify this point, we derive an approximate analytical formula to estimate the polaron formation time t_f (see Supplementary discussion VI [28]). For low damping ($\gamma \ll \omega$), the formation time can be expressed as $t_f = \gamma^{-1} \ln(\tau_{avg}/\Delta_{th})$, where τ_{avg} is the average (absolute) atomic displacement induced by the polaron, Δ_{th} the displacement threshold, and γ the average damping rate. This expression further emphasizes that the polaron formation times are mostly governed by the damping rate γ and by the magnitude of the displacement associated with the formation of a polaron. Using parameters for MgO, we obtain $t_f = 0.7$ ps, in agreement with the ab-initio value of 0.8 ps.

The time dependence of $B_{qv}(t)$ for the LO phonon is further illustrated in Fig. 3 (d) for the wave vectors q_1, q_2 , and q_3 (vertical lines in Fig. 3 (c)), revealing

a structural dynamics characterized by damped oscillations. The Fourier transform of the time series – defined as $B_{qv}(\omega) = \int dt B_{qv}(t) e^{i\omega t}$ and shown in Fig. 3 (e) – yields frequencies in the vicinity of the LO phonon frequencies, thus, identifying this mode with the dominant mechanism behind the fast modulation of the structural distortion. In addition to the LO phonons, however, other frequencies arise that cannot be directly attributed to LO vibrations. To analyze the entire frequency spectrum of the structural oscillations, we define the polaron spectral function as $\mathcal{B}_q^2(\omega) = \sum_{\nu} |B_{qv}(\omega)|^2$. This quantity serves as a global indicator of the vibrational spectrum arising throughout polaron formation, and it can be directly related to the number of phonons contributing to the polaron [24]. The polaron spectral function $\mathcal{B}_q^2(\omega)$ is illustrated in Fig. 4 (a) as a color map as a function of momentum and frequency, while its mode-resolved components $|B_{qv}(\omega)|^2$ are shown in Fig. S6 [28]. The phonon dispersion obtained from DFPT is superimposed for comparison. Here, dark regions indicate the presence of structural oscillations at specific frequencies and momenta, whereas white denotes the absence of oscillatory motion. Oscillations are confined to a well-defined region of momentum space corresponding to the modes actively involved in polaron formation. Most importantly, the frequency spectrum of the polaron differ substantially from the phonon spectrum. In particular, we observe a strong contribution of low-frequency components that have no counterpart in the phonon dispersion. These findings suggest that polaron formation is characterized by distinctive dynamical signatures, which could serve as markers for unambiguously identifying polarons in pump-probe experiments. The difference between the vibrational frequency spectrum of phonons and polarons

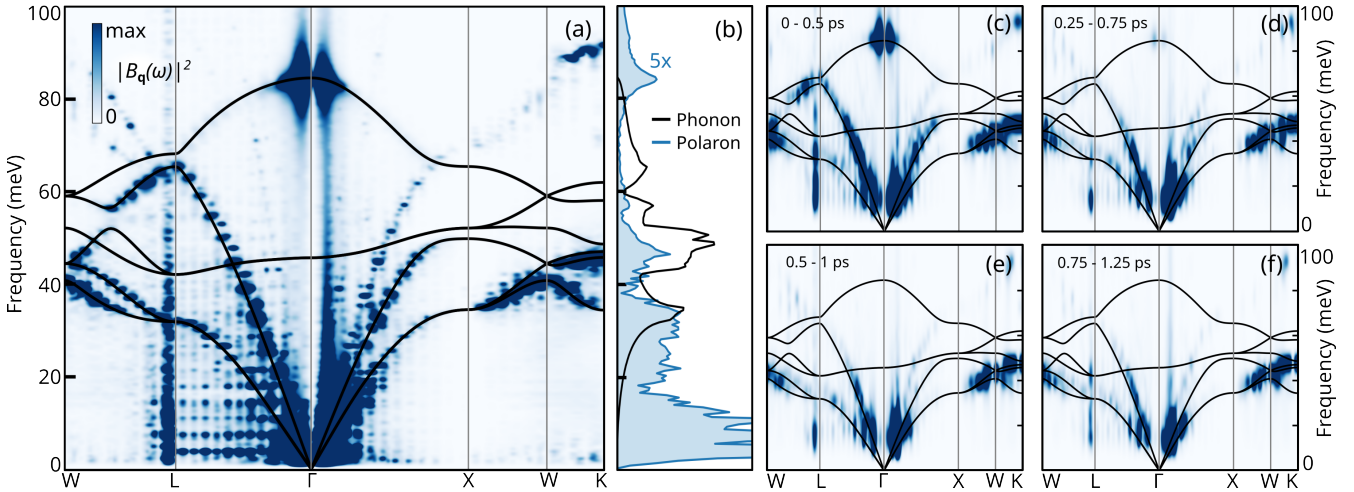


Figure 4. (a) Polaron spectral function $B_q^2(\omega) = \sum_\nu |B_{q\nu}(\omega)|^2$ for momenta along the W-L-Γ-X high-symmetry path. The phonon dispersion obtained from density-functional perturbation theory (black line) is included for comparison. (b) Comparison between the polaron (blue) and the phonon density of state (black). (c-f) Polaron spectral function $B_q^2(\omega)$ obtained by restricting the Fourier transforms to time intervals of 0.5 ps for different time delays after the onset of the dynamics.

is further highlighted in Fig. 4 (b), where the polaron density of states (DOS), defined as $\mathcal{D}_p(\omega) = \int_{\Omega_{BZ}} d\mathbf{q} B_q^2(\omega)$, is compared to the phonon DOS. The decomposition of $\mathcal{D}_p(\omega)$ in its mode-resolved contributions is reported in Fig. S7 [28]. To disentangle the timescales at which different frequency components emerge in the dynamics, Figures 4 (c-f) reports the polaron spectral function $B_q^2(\omega)$ obtained by restricting the Fourier transform to time intervals of 500 fs. This analysis reveals that structural oscillations at the LO frequency only persist throughout the initial phase of polaron formation. In contrast, low-frequency oscillations persist on longer time scales. We attribute these modes to the distinctive vibration dynamics of the polaron that arise from the long-range structural reorganization of the crystal, giving rise to soft vibrational motion absent in the equilibrium cubic structure.

These results offer a guideline for identifying the dynamical fingerprints of polaron formation in pump-probe experiments. In ultrafast diffuse scattering [8], polarons lead to an enhanced scattering intensity in the vicinity of the Bragg peaks [38]. The time-dependent oscillations of the polaron envelop function $B_{q\nu}(t)$ are expected to induce a coherent modulation of this diffuse signal, with a characteristic frequency spectrum as shown in Fig. 4 (a). Importantly, this behavior distinguishes polarons from coherent phonons, which affect only the Bragg peak intensities without generating corresponding features in the diffuse scattering background. The frequency spectrum associated with polaron formation should further leave distinctive signatures in time-resolved optical and ARPES measurements. In presence of polaronic distortions, the band energy $\varepsilon_{n\mathbf{k}}$ is renormalized to $\varepsilon_{n\mathbf{k}} + \Delta\varepsilon_{n\mathbf{k}}(t)$, where $\Delta\varepsilon_{n\mathbf{k}}(t) =$

$N_p^{-1} \sum_{\mathbf{q}\nu} g_{n\mathbf{k}}^\nu(\mathbf{k}, \mathbf{q}) B_{q\nu}(t)$ [21, 39]. Polaron formation can thus be inferred from time-dependent oscillations in the optical or photoemission signal. In particular, the emergence of low-frequency components, typically not associated with coherent phonons, may serve as a distinguishing feature of polaron dynamics, providing a means to separate them from other forms of coherent lattice motion. These considerations provide a rigorous criteria for distinguishing polaron formation from other non-equilibrium phenomena in time-resolved experiments.

In conclusion, we developed a first-principles theoretical framework to describe the ultrafast dynamics of polaron localization. We applied it to investigate the formation of polarons in real time in the polar insulator MgO. Besides estimating the characteristic timescales of polaron localization and decoherence, our simulations reveal a nontrivial dynamical behavior, characterized by damped structural oscillations and a frequency spectrum exhibiting distinctive features beyond those of ordinary harmonic lattice vibrations. These results demonstrate that polaron formation is accompanied by characteristic dynamical fingerprints, which can serve as markers to distinguish polarons from other electronic and vibrational excitations. This insight provides a valuable foundation for interpreting time-resolved pump-probe experiments and for advancing our understanding of nonequilibrium quasiparticle dynamics in polar crystals.

This work was funded by the European Union as part of the MSCA Doctoral Network TIMES (Grant Agreement No. 101118915) and by the Deutsche Forschungsgemeinschaft (DFG), Projects No. 499426961 and 443988403. The authors gratefully acknowledge the computing time provided by the high-performance computer Lichtenberg at the NHR Centers NHR4CES at

TU Darmstadt (Project p0021280). F.C. acknowledges the J. Tinsley Oden Fellowship Research Program of the Oden Institute at the University of Texas Austin. F.G. was supported by the Computational Materials Sciences Program funded by the US Department of Energy, Office of Science, Basic Energy Sciences, under award no. DE-SC0020129. J.L.-B. was supported by Grant No. IT-1527-22, funded by the Department of Education, Universities and Research of the Basque Government, and Grant no. PID2022-137685NB-I00, funded by MCIN/AEI/10.13039/501100011033/ and by “ERDF A way of making Europe”.

[1] C. Franchini, M. Reticcioli, M. Setvin, and U. Diebold, Polarons in materials, *Nat. Rev. Mater.* **6**, 560 (2021).

[2] S. X. Zhang, D. C. Kundaliya, W. Yu, S. Dhar, S. Y. Young, L. G. Salamanca-Riba, S. B. Ogale, R. D. Vispute, and T. Venkatesan, Niobium doped TiO_2 : Intrinsic transparent metallic anatase versus highly resistive rutile phase, *J. Appl. Phys.* **102**, 013701 (2007).

[3] A. D. Wright, L. R. V. Buizza, K. J. Savill, G. Longo, H. J. Snaith, M. B. Johnston, and L. M. Herz, Ultrafast excited-state localization in $Cs_2AgBiBr_6$ double perovskite, *J. Phys. Chem. Lett.* **12**, 3352 (2021).

[4] J. Luo, X. Wang, S. Li, J. Liu, Y. Guo, G. Niu, L. Yao, Y. Fu, L. Gao, Q. Dong, C. Zhao, M. Leng, F. Ma, W. Liang, L. Wang, S. Jin, J. Han, L. Zhang, J. Etheridge, J. Wang, Y. Yan, E. H. Sargent, and J. Tang, Efficient and stable emission of warm-white light from lead-free halide double perovskites, *Nature* **563**, 541 (2018).

[5] H. Liu, A. Wang, P. Zhang, C. Ma, C. Chen, Z. Liu, Y. Zhang, B. Feng, P. Cheng, J. Zhao, L. Chen, and K. Wu, Atomic-scale manipulation of single-polaron in a two-dimensional semiconductor, *Nat. Commun.* **14**, 3690 (2023).

[6] J. Redondo, M. Reticcioli, V. Gabriel, D. Wrana, F. Ellinger, M. Riva, G. Franceschi, E. Rheinfrank, I. Sokolović, Z. Jakub, F. Kraushofer, A. Alexander, E. Belas, L. L. Patera, J. Repp, M. Schmid, U. Diebold, G. S. Parkinson, C. Franchini, P. Kocan, and M. Setvin, Real-space investigation of polarons in hematite Fe_2O_3 , *Sci. Adv.* **10**, eadp7833 (2024).

[7] F. Boschini, M. Zonno, and A. Damascelli, Time-resolved ARPES studies of quantum materials, *Rev. Mod. Phys.* **96**, 015003 (2024).

[8] D. Filippetto, P. Musumeci, R. Li, B. Siwick, M. Otto, M. Centurion, and J. Nunes, Ultrafast electron diffraction: Visualizing dynamic states of matter, *Rev. Mod. Phys.* **94**, 045004 (2022).

[9] K. Miyata, D. Meggiolaro, M. T. Trinh, P. P. Joshi, E. Mosconi, S. C. Jones, F. De Angelis, and X.-Y. Zhu, Large polarons in lead halide perovskites, *Sci. Adv.* **3**, e1701217 (2017).

[10] J. Li, W.-G. Yin, L. Wu, P. Zhu, T. Konstantinova, J. Tao, J. Yang, S.-W. Cheong, F. Carbone, J. A. Misewich, J. P. Hill, X. Wang, R. J. Cava, and Y. Zhu, Dichotomy in ultrafast atomic dynamics as direct evidence of polaron formation in manganites, *npj Quantum Mater.* **1**, 16026 (2016).

[11] H. Seiler, D. Zahn, V. C. A. Taylor, M. I. Bodnarchuk, Y. W. Windsor, M. V. Kovalenko, and R. Ernstorfer, Direct observation of ultrafast lattice distortions during exciton–polaron formation in lead halide perovskite nanocrystals, *ACS Nano* **17**, 1979 (2023).

[12] T. W. Kim, S. Jun, Y. Ha, R. K. Yadav, A. Kumar, C.-Y. Yoo, I. Oh, H.-K. Lim, J. W. Shin, R. Ryoo, H. Kim, J. Kim, J.-O. Baeg, and H. Ihhee, Ultrafast charge transfer coupled with lattice phonons in two-dimensional covalent organic frameworks, *Nat. Commun.* **10**, 1873 (2019).

[13] A. De Sio, F. Troiani, M. Maiuri, J. Réhault, E. Sommer, J. Lim, S. F. Huelga, M. B. Plenio, C. A. Rozzi, G. Cerullo, E. Molinari, and C. Lienau, Watching the coherent birth of polaron pairs in conjugated polymers, *Nat. Commun.* **7**, 13742 (2016).

[14] H.-M. Wang, X.-B. Liu, S.-Q. Hu, D.-Q. Chen, Q. Chen, C. Zhang, M.-X. Guan, and S. Meng, Giant acceleration of polaron transport by ultrafast laser-induced coherent phonons, *Sci. Adv.* **9**, eadg3833 (2023).

[15] W. Chen, T. Wang, C.-C. Yu, Y. Jing, X. Li, and W. Xiong, Small polaron–induced ultrafast ferroelectric restoration in $BiFeO_3$, *Phys. Rev. X* **15**, 021046 (2025).

[16] E. Cinquanta, D. Meggiolaro, S. G. Motti, M. Gandini, M. J. P. Alcocer, Q. A. Akkerman, C. Vozzi, L. Manna, F. De Angelis, A. Petrozza, and S. Stagira, Ultrafast THz probe of photoinduced polarons in lead-halide perovskites, *Phys. Rev. Lett.* **122**, 166601 (2019).

[17] O. Cannelli, N. Colonna, M. Puppin, T. C. Rossi, D. Kinschel, L. M. D. Leroy, J. Löffler, J. M. Budarz, A. M. March, G. Doumy, *et al.*, Quantifying photoinduced polaronic distortions in inorganic lead halide perovskite nanocrystals, *J. Am. Chem. Soc.* **143**, 9048 (2021).

[18] S. Falletta and A. Pasquarello, Many-body self-interaction and polarons, *Phys. Rev. Lett.* **129**, 126401 (2022).

[19] S. Kokott, S. V. Levchenko, P. Rinke, and M. Scheffler, First-principles supercell calculations of small polarons with proper account for long-range polarization effects, *New J. Phys.* **20**, 033023 (2018).

[20] C. Verdi, F. Caruso, and F. Giustino, Origin of the crossover from polarons to Fermi liquids in transition metal oxides, *Nat. Commun.* **8**, 15769 (2017).

[21] J. Lafuente-Bartolome, C. Lian, W. H. Sio, I. G. Gurubay, A. Eiguren, and F. Giustino, Unified approach to polarons and phonon-induced band structure renormalization, *Phys. Rev. Lett.* **129**, 076402 (2022).

[22] J. Lafuente-Bartolome, C. Lian, W. H. Sio, I. G. Gurubay, A. Eiguren, and F. Giustino, Ab initio self-consistent many-body theory of polarons at all couplings, *Phys. Rev. B* **106**, 075119 (2022).

[23] W. H. Sio, C. Verdi, S. Poncé, and F. Giustino, Polarons from first principles, without supercells, *Phys. Rev. Lett.* **122**, 246403 (2019).

[24] W. H. Sio, C. Verdi, S. Poncé, and F. Giustino, Ab initio theory of polarons: Formalism and applications, *Phys. Rev. B* **99**, 235139 (2019).

[25] A. S. Mishchenko, N. V. Prokof’ev, A. Sakamoto, and B. V. Svistunov, Diagrammatic quantum Monte Carlo study of the Fröhlich polaron, *Phys. Rev. B* **62**, 6317 (2000).

[26] Y. Luo, J. Park, and M. Bernardi, First-principles diagrammatic monte carlo for electron–phonon interactions and polaron, *Nature Physics* 10.1038/s41567-025-02954-1

(2025).

[27] F. Giustino, Electron-phonon interactions from first principles, *Rev. Mod. Phys.* **89**, 015003 (2017).

[28] See Supplemental Material at <https://link.aps.org/supplemental/10.1103/PhysRevLett.XXX.YYYY> for [brief description of what the supplement contains] and additional citations to Refs. [? ? ? ? ?], Supplemental Material.

[29] Y. Pan, C. Emeis, S. Jauernik, M. Bauer, and F. Caruso, Origin of phonon decoherence (2025), arXiv:2502.01529.

[30] H. Lee, S. Poncé, K. Bushick, S. Hajinazar, J. Lafuente-Bartolome, J. Leveilée, C. Lian, J.-M. Lihm, F. Macheda, H. Mori, H. Paudyal, W. H. Sio, S. Tiwari, M. Zacharias, X. Zhang, N. Bonini, E. Kioupakis, E. R. Margine, and F. Giustino, Electron-phonon physics from first principles using the EPW code, *npj Comput. Mater.* **9**, 156 (2023).

[31] S. Chae, N. Sanders, K. A. Mengle, A. Wang, X. Zhang, J. L. Bartolome, K. Luo, Y.-C. Huang, F. Giustino, J. T. Heron, and E. Kioupakis, Extreme-band-gap semiconductors with shallow dopants and mobile carriers (2025), arXiv:2506.07284.

[32] S. Baroni, S. de Gironcoli, A. Dal Corso, and P. Giannozzi, Phonons and related crystal properties from density-functional perturbation theory, *Rev. Mod. Phys.* **73**, 515 (2001).

[33] P. Giannozzi, O. Andreussi, T. Brumme, O. Bunau, M. B. Nardelli, M. Calandra, R. Car, C. Cavazzoni, D. Ceresoli, M. Cococcioni, *et al.*, Advanced capabilities for materials modelling with **Quantum ESPRESSO**, *J. Phys. Condens. Matter* **29**, 465901 (2017).

[34] B. Sadigh, P. Erhart, and D. Åberg, Variational polaron self-interaction-corrected total-energy functional for charge excitations in insulators, *Phys. Rev. B* **92**, 075202 (2015).

[35] Z. Dai, D. Kim, J. Lafuente-Bartolome, and F. Giustino, Comparison between first-principles supercell calculations of polarons and the ab initio polaron equations (2025), arXiv:2511.01764 [cond-mat.mtrl-sci].

[36] B. Wu, W. Ning, Q. Xu, M. Manjappa, M. Feng, S. Ye, J. Fu, S. Lie, T. Yin, F. Wang, *et al.*, Strong self-trapping by deformation potential limits photovoltaic performance in bismuth double perovskite, *Science Advances* **7**, eabd3160 (2021).

[37] S. A. Bretschneider, I. Ivanov, H. I. Wang, K. Miyata, X. Zhu, and M. Bonn, Quantifying polaron formation and charge carrier cooling in lead-iodide perovskites, *Advanced Materials* **30**, 1707312 (2018).

[38] T. L. Britt, F. Caruso, and B. J. Siwick, A momentum-resolved view of polaron formation in materials, *npj Comput. Mater.* **10**, 178 (2024).

[39] C. Emeis, S. Jauernik, S. Dahiya, Y. Pan, C. E. Jensen, P. Hein, M. Bauer, and F. Caruso, Coherent Phonons and Quasiparticle Renormalization in Semimetals from First Principles, *Phys. Rev. X* **15**, 021039 (2025).